

Supplementary Materials for

Soil organic matter attenuates the efficacy of flavonoid-based plant-microbe communication

Ilenne Del Valle*, Tara M. Webster*, Hsiao-Ying Cheng, Janice E. Thies, André Kessler, Mary Kaitlyn Miller, Zachary T. Ball, Kevin R. MacKenzie, Caroline A. Masiello, Jonathan J. Silberg, Johannes Lehmann

*Corresponding author. Email: idd1@rice.edu (I.D.V.); tara.webster@colorado.edu (T.M.W.)

Published 29 January 2020, *Sci. Adv.* **6**, eaax8254 (2020)
DOI: 10.1126/sciadv.aax8254

This PDF file includes:

Fig. S1. Structures of flavonoids.

Fig. S2. Experimental protocols for determining the effects of soils and amendments on naringenin.

Fig. S3. Naringenin bioavailability as a function of soil physiochemical properties.

Fig. S4. Naringenin bioavailability is decreased by POC_{plant} but not by PyOM.

Fig. S5. Naringenin bioavailability is not changed by oxidized PyOM.

Fig. S6. Manganese dioxide mediates a reaction between catechin and naringenin.

Fig. S7. Chromatograms of naringenin and EDTA.

Fig. S8. Mass spectrum acquired for naringenin and EDTA.

Fig. S9. Chromatograms of DOC_{ac} and DOC_{pp}.

Fig. S10. Partial chromatograms of DOC_{ac} after the addition of EDTA in the presence or absence of naringenin.

Fig. S11. Bonding topologies of DOC_{pp} and naringenin heterodimers.

Text S1. Structural determination using ¹H and ¹³C NMR spectra.

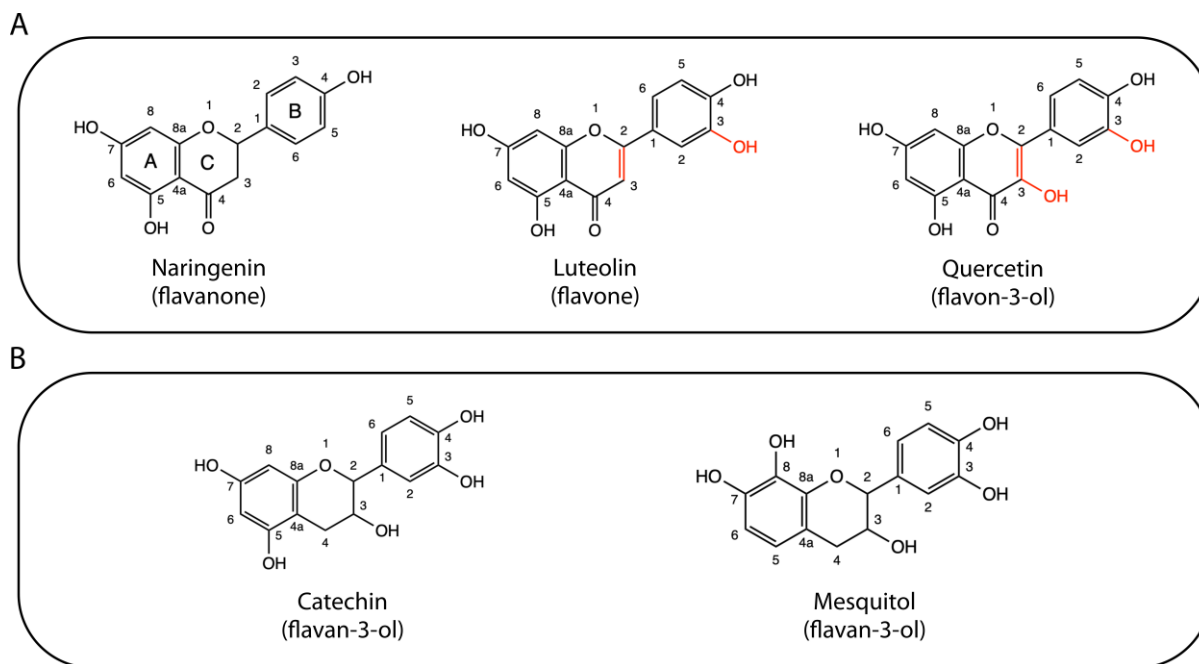


Fig. S1. Structures of flavonoids. (A) Naringenin, luteolin, and quercetin structures. In naringenin, the A, B, and C rings in the carbon skeleton are labeled. In luteolin and quercetin, their additional hydroxyl groups and double bonds are shown in red. (B) Potential flavan-3-ols present in DOC_{plant}.

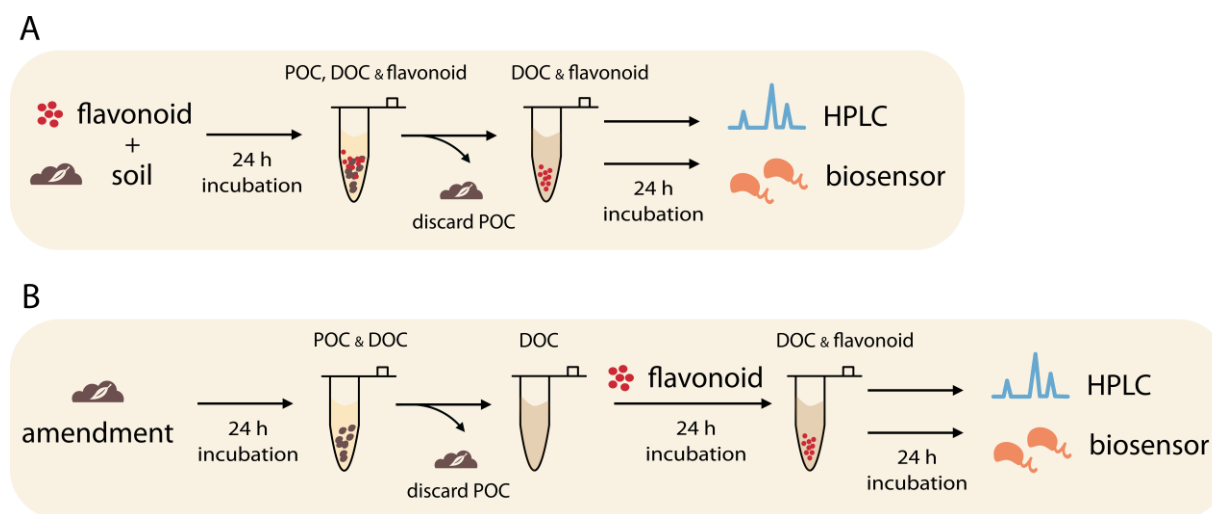


Fig. S2. Experimental protocols for determining the effects of soils and amendments on naringenin. In all cases, each soil or amendment (POC) was first incubated in phosphate buffer (10 mM, pH = 7). (A) Flavonoids were added to the POC/buffer mixture and incubated for 24 h. Samples were subsequently centrifuged, and then flavonoid remaining in the supernatant was quantified using the HPLC or using the biosensor. In the case of the biosensor, the supernatant was mixed at a ratio of 1:1 with a culture of biosensor cells and incubated for 24 h at 30°C prior to measuring reporter levels. (B) To study DOC effects on flavonoids, POC was separated from the supernatant (DOC), DOC was incubated with naringenin for 24 h, and then the amount of flavonoid remaining was quantified using HPLC or biosensor as described above.

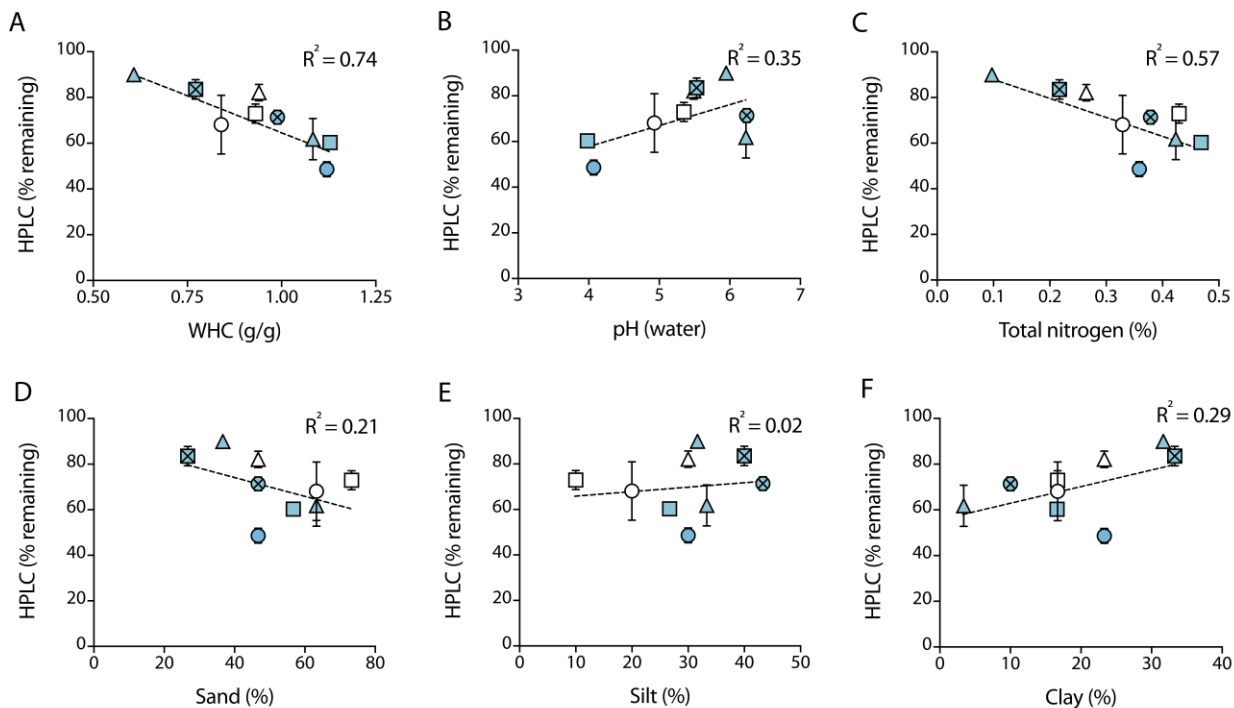


Fig. S3. Naringenin bioavailability as a function of soil physiochemical properties.

Inceptisols from three different sites (square, triangle and circle) and three different land uses (agriculture = crossed circle, meadow = open circle, and forest = filled circle) were incubated with $75 \mu\text{M}$ naringenin for 24 h and then analyzed using HPLC. The naringenin peak area obtained following each soil incubation is plotted versus (A) water holding capacity of the soil (g water g^{-1} soil), (B) soil pH, (C) total nitrogen contents, and (D, E, F) the proportion of sand, silt and clay respectively. Error bars represent $\pm 1\sigma$ calculated using $n = 3$ for each site and land use type.

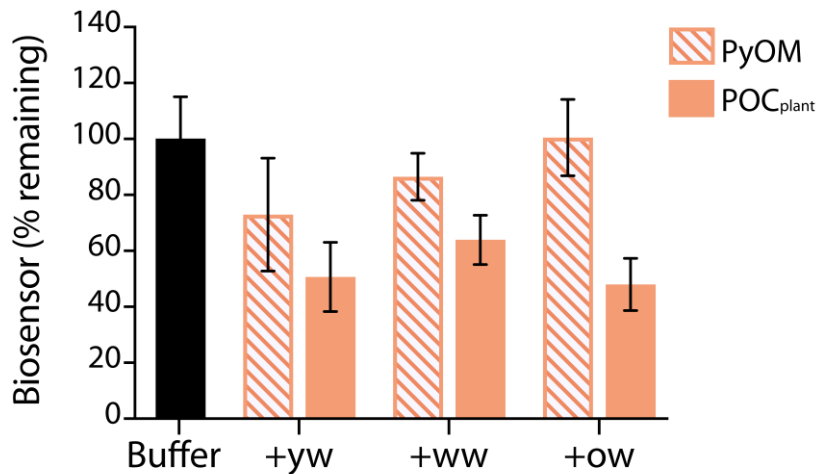


Fig. S4. Naringenin bioavailability is decreased by POC_{plant} but not by PyOM. Naringenin (150 μ M) was incubated in direct contact with POC_{plant} from different sources, including yard waste (yw), wood waste (ww), and oak wood (oc) feedstocks (solid orange) or their corresponding PyOM generated at 550°C (dashed orange). Positive control (buffer only) is shown in black. Samples were centrifuge, supernatant was diluted two-fold with the naringenin biosensor such that the final maximum naringenin concentration was 75 μ M, and the mixture was incubated for 24 h prior to measuring fluorescence. Background corrected fluorescence was normalized by cell growth and used to estimate the % naringenin remaining in solution. Error bars represent $\pm 1\sigma$ calculated using a $n = 3$.

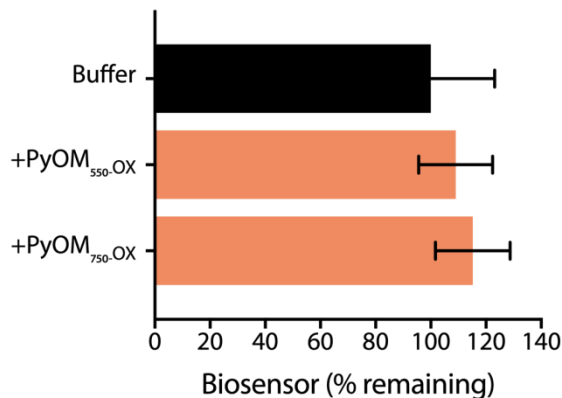


Fig. S5. Naringenin bioavailability is not changed by oxidized PyOM. Maple biochar pyrolyzed at 550°C (+PyOM_{550-OX}) and 750°C (+PyOM_{750-OX}) were oxidized with hydrogen peroxide by mixing 30 g of each biochar with 400 mL of 22.5% hydrogen peroxide for 24 hours, then washing with MilliQ water, and repeating a second time with fresh hydrogen peroxide. Naringenin (0.6 mM) was incubated in direct contact with oxidized PyOM. Samples were centrifuged, and the supernatant was diluted two-fold with the naringenin biosensor such that the final maximum naringenin concentration was 0.3mM. The mixture was incubated for 24 h prior to measuring fluorescence. Background corrected fluorescence was normalized by cell growth and used to estimate the % naringenin remaining in solution. Positive control (buffer only) is shown in black. Error bars represent $\pm 1\sigma$ calculated using a $n = 3$. No significant difference was observed between the buffer control and the samples incubated with oxidized PyOM [one-way analysis of variance (ANOVA) with Dunnett's multiple comparisons test, $*P < 0.005$ and $**P < 0.001$].

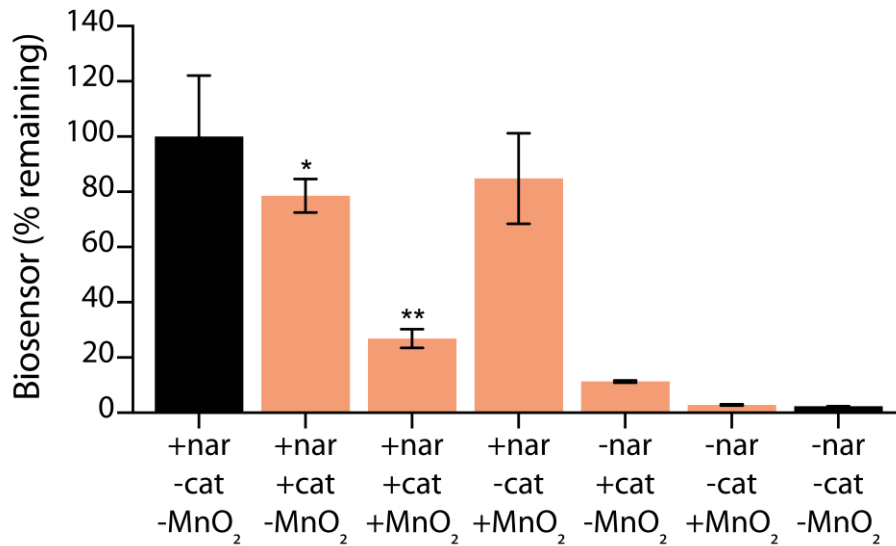


Fig. S6. Manganese dioxide mediates a reaction between catechin and naringenin. A defined concentration of 0.6 mM naringenin (nar) was incubated in the presence (+) or absence (-) of 0.6 mM catechin (cat) and manganese dioxide (MnO₂) for 24 h at 30°C. Samples were centrifuged, and supernatant was incubated for an additional 24 h at 30°C with the naringenin biosensor following a 1:1 dilution of the supernatant. Background corrected fluorescence was normalized by cell growth and used to estimate the proportion of naringenin remaining in solution. An unpaired t-test was used to compare the positive control for naringenin alone (+nar) with the mixture of catechin (+nar+cat) and the mixture of catechin and MnO₂ (+nar+cat+MnO₂; * p<0.005 and ** p<0.001). Error bars represent ±1σ calculated from a n = 3.

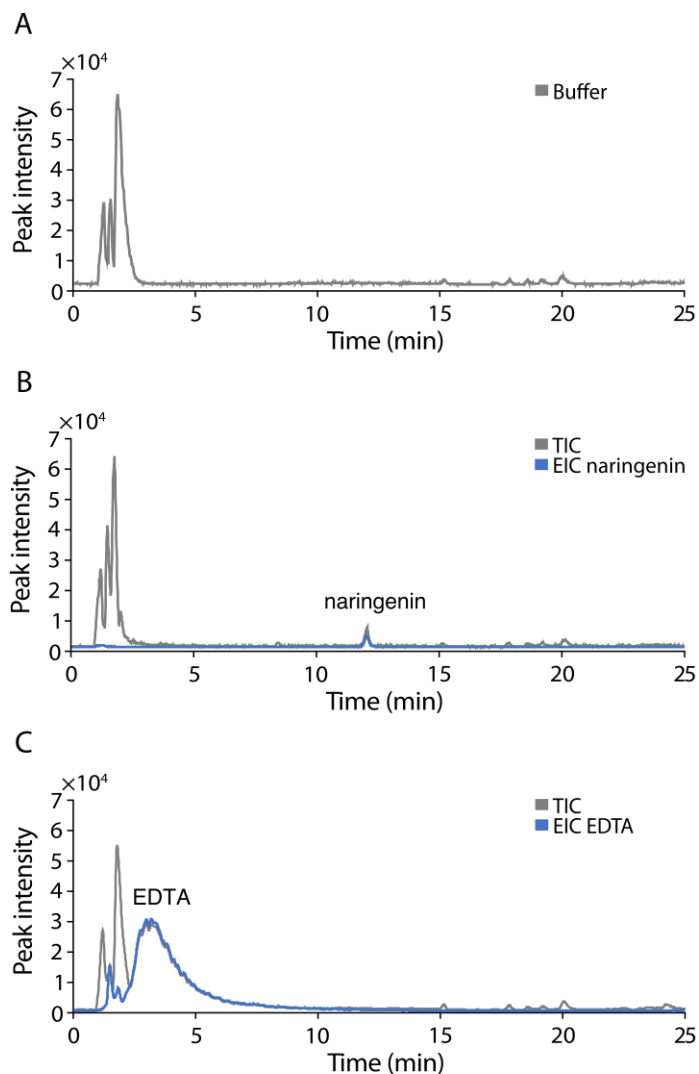


Fig. S7. Chromatograms of naringenin and EDTA. Full chromatograms of the different LC-MS controls, including: (A) 10 mM phosphate buffer at pH 7, (B) buffer after addition of 30 μ M naringenin, which shows the appearance of a peak of retention time (RT) of 12.1 min, and (C) buffer after addition of 1 mM of EDTA, showing a peak with a RT of 2.3 min. The total ion chromatograms (TICs) are shown in grey, while the extracted ion chromatograms (EICs) for naringenin (273 m/z) and EDTA (293 m/z) are shown in blue.

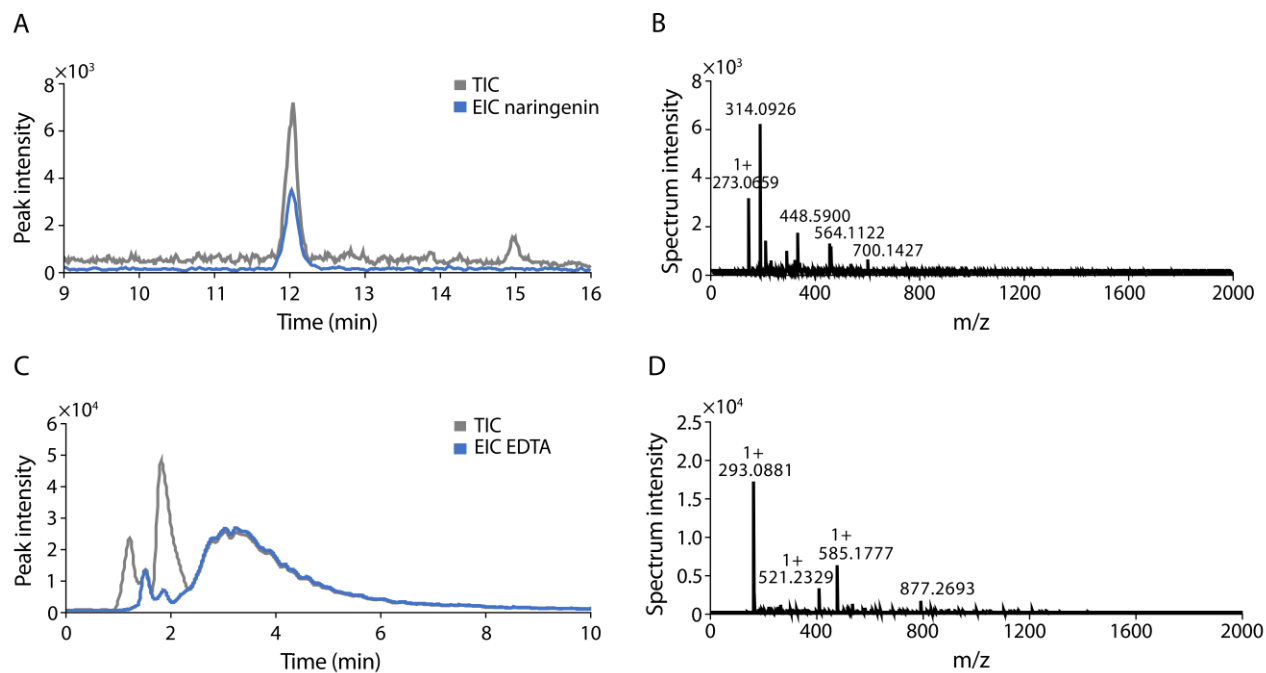


Fig. S8. Mass spectrum acquired for naringenin and EDTA. Close up of the TICs (grey) and EICs for (A) naringenin (B) and EDTA. Mass spectra acquired for (C) the naringenin peak at 12.1 min ($m/z = 273.0659$) and (D) EDTA peak at 2.3 min ($m/z = 293.0881$). Major fragmentation peaks are labeled. 1+ indicates positive ionization mode [M+1].

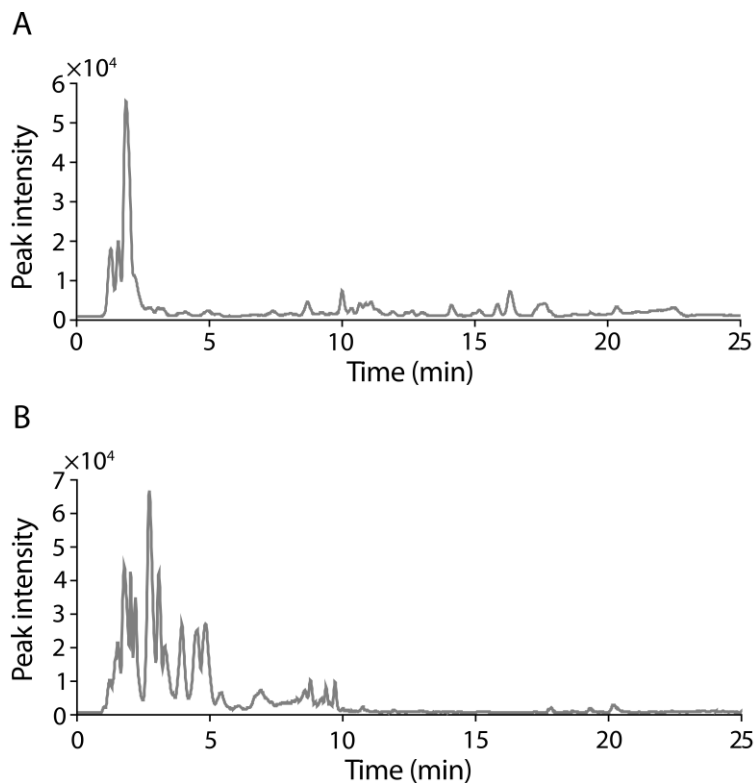


Fig. S9. Chromatograms of DOC_{ac} and DOC_{pp} . POC_{plant} (25 mg mL^{-1}) was incubated for 24 h at 30°C in 10 mM phosphate buffer $\text{pH} = 7$, and the supernatant was removed and evaluated using LC-MS. The total ion chromatograms of DOC from (A) maple (DOC_{ac}) and (B) mesquite wood (DOC_{pp}).

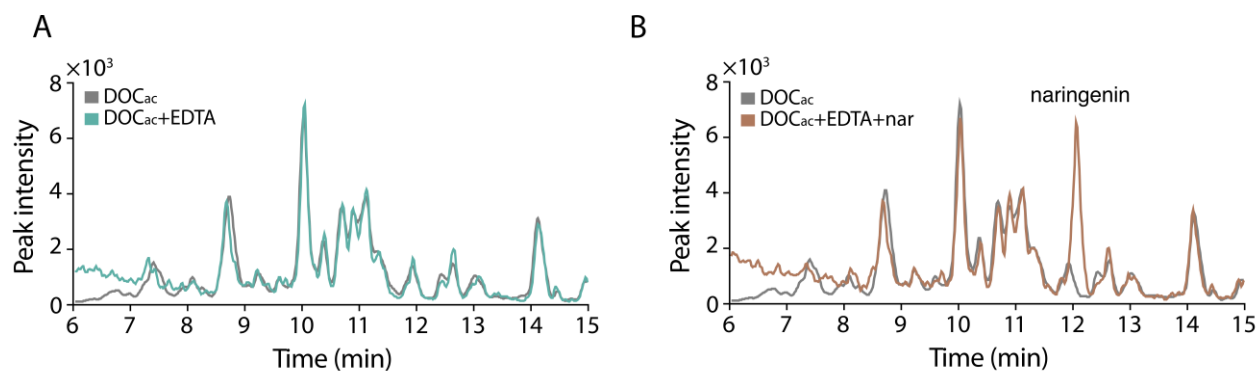


Fig. S10. Partial chromatograms of DOC_{ac} after the addition of EDTA in the presence or absence of naringenin. POC_{plant} (25 mg mL⁻¹) was incubated for 24 h at 30°C in 10 mM phosphate buffer, and the supernatant was separated by centrifugation to obtain DOC_{ac}. DOC_{ac} (grey) is compared with (A) DOC_{ac} after addition of 1 mM EDTA and incubation for 24 h (green), and (B) DOC_{ac} after addition of 1 mM EDTA and 30 μ M of naringenin and incubation for 24 h (brown). With the EDTA treatment, no differences were observed between the peaks before and after chelator addition, indicating that naringenin does not interact directly with DOC_{ac}. In the presence of EDTA and naringenin, the peak observed in Fig. 4A (RT = 10.7 min) is no longer observed.

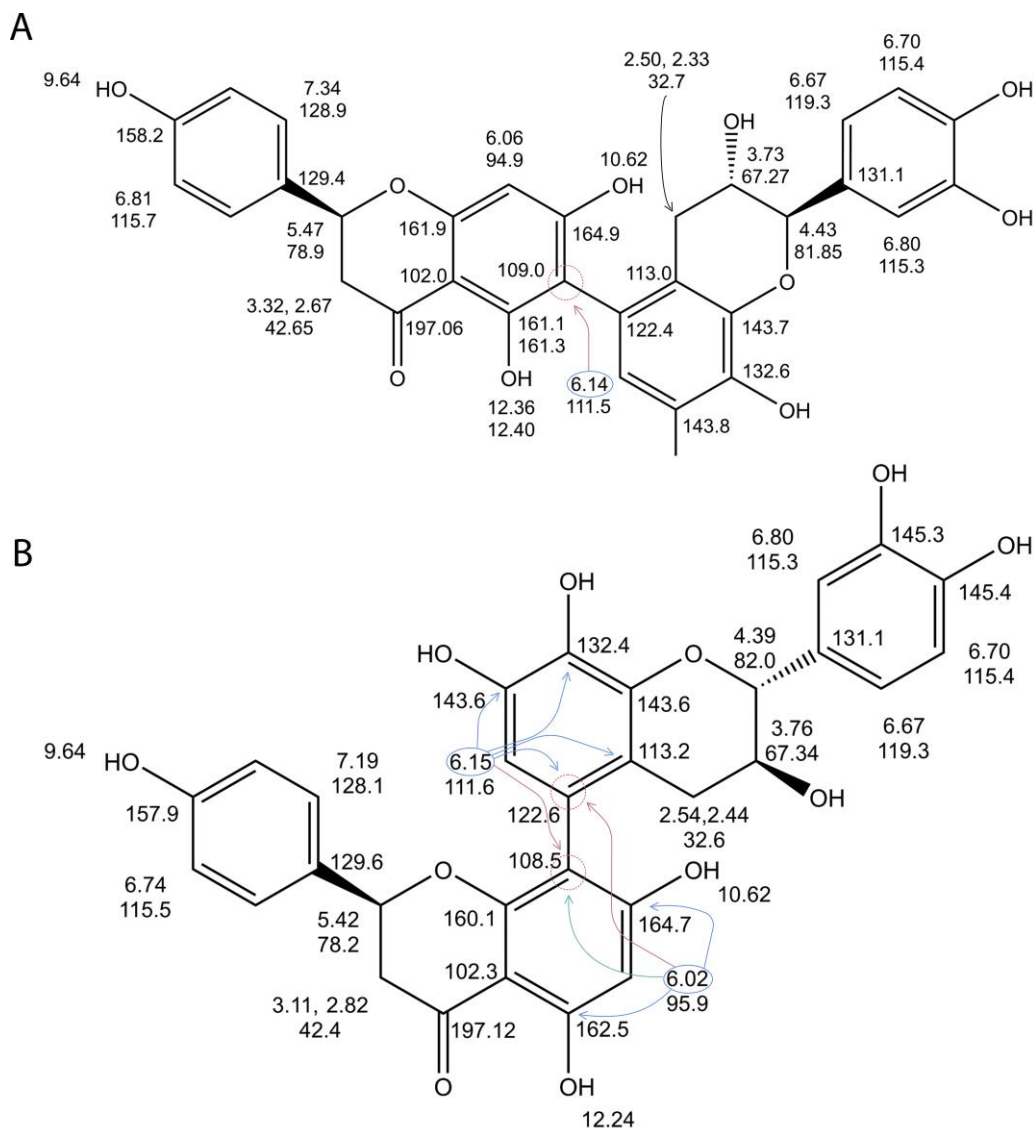


Fig. S11. Bonding topologies of DOC_{pp} and naringenin heterodimers. NMR structure of chemicals isolated from DOC_{pp} following incubation with naringenin. **(A)** Structure of mesquitol-C(5)-C(6)-naringenin and **(B)** mesquitol-C(5)-C(8)-naringenin heterodimers. All arrows represent peaks found in the HMBC spectrum that correlate a hydrogen chemical shift with a carbon chemical shift (*see* Supplementary Text 1).

Text S1. Structural determination using ^1H and ^{13}C NMR spectra. The parent compound naringenin has a downfield phenolic hydrogen (H5, 12.16 ppm) that shows multiple bond correlations to the naringenin A ring carbons in the HMBC spectra acquired in DMSO. HMBC peaks at ^{13}C shifts of 96.3, 102.2, 163.9, and 167.1 ppm correspond to C6, C10, C7, and C5 (respectively), and a very weak peak at 196.8 ppm indicates C4. We used these (and other) long range heteronuclear correlations to identify sites of chemical changes to the naringenin core. NMR spectra in DMSO reveal three related sets of downfield protons in the 12.2-12.45 ppm range that show many HMBC correlations; the presence of these ^1H resonances and ^{13}C correlations suggest that naringenin-like species may be present. Major peaks at 12.41 and 12.36 ppm show HMBC correlations at shifts of 102.0, 109.0, 161.2, and 164.8 ppm. The lack of a correlation at ~96 ppm and the presence of a correlation at 109.0 ppm indicates that C6 of this molecule has been modified (relative to naringenin); the ‘new’ carbon at 109.0 ppm does not have an attached proton.

The spectra contain a number of resonances belonging to spin systems unrelated to naringenin. Based on the mass of the products, we reasoned that these might be derived from mesquitol, a reactive flavonoid found in wood. HSQC and HMBC correlations confirm the presence of a mesquitol-like molecular topology, except that the mesquitol C5 position lacks an attached proton, implicating this as the reactive site. The mesquitol-like H6 shows a strong HMBC correlation at 109.0 ppm, the ‘new’ shift detected in the naringenin-like spin system described above. These correlations establish the molecular topology shown in fig. S10A. Close inspection of the HMBC correlations for the naringenin-like H8 hydrogen reveals a weak correlation to 122.4 ppm; this four-bond coupling is possible because of ‘W’ geometry (‘W’ correlations to the naringenin-like carbonyl at 197.1 ppm are also detected). Two peaks are detected for most resonances associated with this topology, likely because of atropisomerism: the joined aromatic rings can take either of two chiral propeller twists that exchange slowly due to steric hindrance, and the presence of chiral centers in the parent molecules makes these diastereomers.

A major peak at 12.24 ppm shows HMBC correlations at shifts of 95.9, 102.3, 162.5, and 164.7 ppm, consistent with carbons 6, 10, 7, and 5 retaining their chemical identity in this molecule. HMBC correlations to H6 reveal the loss of a characteristic 95 ppm shift, indicating that C8 has been modified. H6 shows HMBC correlations at two new ^{13}C shifts, 108.5 and 122.6 ppm, neither of which has an attached proton. Further analysis of HMBC correlations determines the molecular topology shown in fig. S10B. The resonances associated with this topology also show evidence of atropisomerism.

The identification of the bonding topologies for these major species visible by NMR does not eliminate the possibility that other molecular topologies may be represented at low abundance.